Surface and dynamic structures of bacteriorhodopsin in a 2D crystal, a distorted or disrupted lattice, as revealed by site-directed solid-state ^{13}C NMR

Hazime Saitô,[1,2*] Yasuharu Kawase,[1] Atushi Kira,[1] Kazutoshi Yamamoto,[1] Michikazu Tanio,[1] Satoru Yamaguchi,[1] Satoru Tuzi[1] and Akira Naito[3]

[1]Department of Life Science, Himeji Institute of Technology, University of Hyogo, Harima Science Garden City, Kouto 3-chome, Kamigori, Hyogo, Japan 678-1297,

[2]Center for Quantum Life Sciences, Hiroshima University, Kagamiyama 1-chome, Higashi-Hiroshima, Japan 739-8526,

[3]Graduate School of Engineering, Yokohama National University, Tokiwadai, Hodogaya-ku, Yokohama, Japan

*Address correspondence to: #203, 3-15-21 Sumiyoshi-honmachi, Higashinada-ku, Kobe, Japan 658-0051, Fax +81-78-856-2876

E-mail address: hsaito@siren.ocn.ne.jp

ABSTRACT

The 3D structure of bacteriorhodopsin (bR) obtained by x-ray diffraction or cryo-electron microscope studies is not always sufficient for a picture at ambient temperature where dynamic behavior is exhibited. For this reason, a site-directed solid-state ^{13}C NMR study of fully hydrated bR from purple membrane (PM), or a distorted or disrupted lattice, is very valuable in order to gain insight into the dynamic picture. This includes the surface structure, at the *physiologically important* ambient temperature. Almost all of the ^{13}C NMR signals are available from [3-^{13}C]Ala or [1-^{13}C]Val-labeled bR from PM, although the ^{13}C NMR signals from the surface areas, including loops and transmembrane α-helices near the surface (8.7Å depth), are suppressed for preparations labeled with [1-^{13}C]Gly, Ala, Leu, Phe, Tyr, etc. due to a failure of the attempted peak-narrowing by making use of the interfered frequency of the frequency of fluctuation motions with the frequency of magic angle spinning. In particular, the C-terminal residues, 226-235, are present as the C-terminal α-helix which is held together with the nearby loops to form a surface complex, although the remaining C-terminal residues undergo isotropic motion even in a 2D crystalline lattice (purple membrane) under physiological conditions. Surprisingly, the ^{13}C NMR signals could be further suppressed even from [3-^{13}C]Ala- or [1-^{13}C]Val-bR, due to the acquired fluctuation motions with correlation times in the order of 10^{-4} to 10^{-5} s, when the 2D lattice structure is instantaneously distorted or completely disrupted, either in photo-intermediate, removed retinal or when embedded in the lipid bilayers.

INTRODUCTION

Bacteriorhodopsin (bR) is a light-driven proton pump from *Halobacterium salinarum.* It assembles into naturally occurring 2D crystalline patches known as purple membrane (PM) in which its trimeric unit is hexagonally packed (1-7) to form PM under physiological conditions. Many integral membrane proteins in the membrane environment are also known to assemble into oligomeric complexes rather than monomers to lead to tertiary and quarternary structures as revealed by x-ray diffraction or cryo-electron microscope studies. This has been demonstrated for chloride pump halorhodopsin (8,9), phototaxis receptor sensory rhodopsin II (10-12), a photosynthetic reaction center (13), a light-harvesting complex (14,15), cytochrome c oxidase (16,17), potassium and mechanosensitive channels (18,19), bovine rhodopsin (20), the calcium pump of sarcoplasmic reticulum (21), etc. This is because the conformation and dynamics of such membrane proteins as determined by x-ray diffraction or cryo-electron microscope studies are mainly regulated by specific lipid-protein and protein-protein interactions with the surrounding lipids and neighboring proteins as structural determinants, especially those leading to a 2D assembly in bR (22).

Nevertheless, the surface structure data of many such proteins, including bR, are still missing, either obscured or inconsistent, among a variety of 3D structures as revealed by cryo-electron microscopy and X-ray diffraction studies (3-7). These could be biologically very important, providing information on the transport and signal transduction of these proteins. In addition, it appears that such biological activities are retained also in a monomeric form present as solubilized in detergents or reconstituted in lipid bilayers, rather than in a crystalline or oligomerized form. Indeed, the functional unit of bR, as a naturally occurring 2D crystal as PM which is responsible for the

photocycle, is the monomer itself (23-25). However, the lifetimes of the L and N intermediates are significantly shorter than in the monomer (26,27). Therefore, a plausible conformation and dynamic change during conversion from the 2D crystal to an instantaneous monomeric structure may also play an important role for its biological activity.

The site-directed ^{13}C NMR approach on *selectively* ^{13}C-labeled membrane proteins from either the 2D crystalline state or the monomer turn out to be a very valuable, alternative means revealing conformational features as well as the dynamics of *whole areas* of *fully hydrated* proteins *at ambient temperature*. This includes the surface residues arising from both the N- or C-terminal residues as well as the interhelical loops. We briefly describe here the surface and dynamic structures of fully hydrated bR in the 2D crystal. The distorted or disrupted lattice can be evaluated with respect to its relation to its biological function, as revealed by site-directed ^{13}C NMR. Understanding of such pictures is crucially important, as a reference, for interpretation of the ^{13}C NMR data on a variety of membrane proteins reconstituted in lipid bilayers.

SITE-DIRECTED ^{13}C NMR APPROACH ON BR FROM 2D CRYSTAL

X-ray and cryo-electron microscopic studies have yielded considerable structural information about the intramembrane portion of bR but little is known about the disposition of the loops and the N- or C-terminus (2-7). The transmembrane α-helices thus obtained are shown in the boxes as demonstrated in the schematic representation of the primary structure of bR taking into account its secondary structure (Figure 1) (3,5). The remaining portions are flexible enough to allow a variety of fluctuation motions with various ranges of correlation time from 10^{-4} to 10^{-9} s (28-32). This is because some

3D crystal packing of bR may limit the conformational flexibility of the loops, while the surface in the 2D crystals is not hindered by 3D contacts (33,34).Therefore, a number of *fully hydrated* membrane proteins of biological relevance are far from rigid bodies even in a 2D crystal or monomeric state, at least at *ambient temperature.*

Appropriate isotopic enrichment (labeling), as high as possible approaching to 100 %, is essential for solid-state ^{13}C NMR studies of membrane proteins, in order to enhance both the *sensitivity* and the *selectivity* of their labeled signals from the background signals arising from residues of natural ^{13}C abundance. However, it is cautioned that ^{13}C NMR signals from portions undergoing fast isotropic, fluctuation motions such as the N- or C-terminal residues of bR (with a correlation time shorter than 10^{-8} s) are preferentially suppressed by cross polarization-magic angle spinning (CP-MAS) NMR. This is because the ^{13}C magnetizations from such regions, generated by ^{13}C-^{1}H dipolar interactions, are completely time-averaged by isotropic fluctuation motions. In such cases, the corresponding ^{13}C NMR spectra can be conveniently recorded by an alternative, dipolar decoupled magic angle spinning (DD-MAS) NMR experiments (28,29). Here we compare the ^{13}C DD-MAS and CP-MAS NMR spectra of fully hydrated [3-^{13}C]Ala-labeled bR from PM (centrifuged pellet) as a 2D crystal (Figure 2A and B, respectively) (35). Up to twelve ^{13}C NMR signals, including contributions fom the five single carbon signals among 29 Ala residues in bR (see Figure 1 for the location of the individual Ala residues), are well-resolved in the two types of spectra. The three intense ^{13}C NMR signals marked by gray in the DD-MAS NMR spectrum (Figure 2A) are significantly suppressed in the corresponding CP-MAS NMR spectrum (Figure 2B). These suppressed peaks in the latter are obviously ascribed to the N- or C-terminal regions protruding from the membrane surface which undergo

fast isotropic fluctuation motions with correlation times shorter than 10^{-8} s (28,29). Only three peaks could be resolved, however, when lyophilized preparations were used instead of the fully hydrated pelleted samples currently used (36).

The presence of the picosecond internal motions of the fully hydrated bR/lipid complex was also revealed by neutron scattering studies (37). It appears that the above-mentioned N- or C-terminal residues, rather than the major transmembrane α-helices, are responsible for such fast thermal fluctuations detected by the neutron diffraction. These are from small-amplitude atomic and molecular vibrations up to large-amplitude stochastic reorientational motions of the molecular subunit, which are not hindered by any crystal contacts. Indeed, water molecules "lubricate" such picosecond motions and the light-triggered micro- to millisecond tertiary structural changes of the protein (38). In addition, the lipids and their ability to attract solvent molecules play an important role in producing such hydration-induced flexibility. Thus, *well-resolved ^{13}C NMR spectra are available from the fully hydrated, intact proteins under physiological conditions.*

Spectral resolution of uniformly or extensively ^{13}C-labeled proteins, however, might be desperately deteriorated, if a directly bonded ^{13}C-^{13}C sequence is present in the dense ^{13}C spin networks. If fluctuation motions with correlation times from 10^{-4} to 10^{-5} s are present, as described later, these are manifested by the extremely broadened ^{13}C CP-MAS NMR spectra of [1,2,3-$^{13}C_3$]Ala- labeled bR from PM (39). This is the reason why site-directed or amino-acid-selective isotope labeling is favorable for membrane proteins to avoid such dense ^{13}C spin-networks.

SITE-DIRECTED ASSIGNMENT OF PEAKS

A specific peak, with reduced ^{13}C peak-intensity, from a site-directed mutant, in which an amino-acid residue is replaced by another residue, can be assigned to the residue of interest with reference to that of the wild-type. Here, we assume that any additional spectral change owing to an accompanying conformational change can be neglected. For instance, the Ala C_β ^{13}C NMR peaks of Ala 196 (F-G loop) and Ala 126 (at the corner of the helix D) of [3-^{13}C]Ala-labeled bR are straightforwardly assigned to the peaks suppressed in the site-directed mutants, A196G and A126G, respectively (see Figure 2 for the assigned peaks). Because no additional spectral change is noted upon the introduction of such site-directed mutagenesis (35). A variety of selectively ^{13}C labeled amino-acid residues can be utilized for this purpose. It is cautioned, however, that several ^{13}C NMR signals could be missing from the site(s) of ^{13}C-labeling, depending upon their locations and samples (2D crystal or monomer). Therefore, a prior knowledge is required as to whether or not the incorporated ^{13}C NMR signals are fully visible from the site(s). It is shown that the^{13}C NMR signals for Ala C_β are almost fully visible from the fully hydrated [3-^{13}C]Ala-labeled bR from PM at ambient temperatures (40).

In many instances, however, more complicated spectral changes could be induced in the difference spectrum between the wild type and the site-directed mutant. These are due to local conformational changes accompanied by site-directed mutagenesis, yielding several sets of dispersion peaks (41). To remove such undesirable dispersion peaks, Tuzi et al. have proposed a powerful means to eliminate such dispersion peaks from the surface areas by accelerated Mn^{2+}-induced ^{13}C transverse relaxation (42,43). This is applicable to those residues giving disturbing signals which are mainly located near the surface areas, or a residue of interest is located within the transmembrane helices as in

A215G, A81G, A184G, A53G, etc. (44). The assigned peaks thus obtained can be used as a very convenient probe to examine the *local conformation* of the residues under consideration, with reference to the data base of the conformation- dependent displacement of ^{13}C chemical shifts (28,29,45,46). As to the ^{13}C NMR signals of [3-^{13}C]Ala-bR, two kinds of α-helices, α_I- and α_{II}-helices, are conveniently distinguished as viewed from their peaks with reference to those of $(Ala)_n$ in the solid and in a hexafluoroisopropanol (HFIP) solution, respectively. The concept of the α_{II} helix was initially proposed by Krimm and Dwivedi based on their infrared study (47) and later extended to the interpretation of the ^{13}C chemical shifts utilizing their sample system (40).

This approach is not always successful for the assignment of peaks from several [3-^{13}C]Ala-labeled proteins. However, it is applicable when several peaks are simultaneously displaced or suppressed, owing to induced global conformational changes of the proteins by a site-directed mutagenesis, as encountered for the D85N mutant of bR (48). In such cases, use of [1-^{13}C]Val-labeled proteins rather than [3-^{13}C]Ala-D85N turned out to be more useful (48,49), because this label is in some instances less sensitive to such conformational changes.

RESIDUE-SPECIFIC DYNAMICS OF BR IN 2D CRYSTAL

Surprisingly, the ^{13}C NMR signals turn out to be not always fully visible, especially from the surface areas of membrane proteins undergoing local fluctuation motions, in spite of the 2D crystalline preparations of bR from PM (40,41). To clarify this problem, a relative contribution to the ^{13}C NMR signals (*f*) from residues located near the surface areas was evaluated by comparing their peak-intensities in the presence (*I*) with those in

the absence of 40 μM Mn^{2+} (I_0),

$$f = 1 - I/I_0. \quad (1)$$

The relative contributions of the ^{13}C NMR signals from the surface areas (I_0-I) can be defined as residues located within 8.7 Å from the membrane surface (44), because these ^{13}C NMR signals from the residues within these areas can be completely suppressed (giving rise to a line width larger than 100 Hz) by the accelerated transverse relaxation process caused by the Mn^{2+} ion (42,43) (see Table I). Alternatively, the proportion of such residues near the surface (8.7 Å from the membrane surface; see the gray area in Figure 1), g, can be easily counted by examination of the primary sequence of bR taking into account its secondary structure (see Figure 1),

$$g = n/n_0 \quad (2)$$

where n and n_0 are the number of residues concerned located within such areas (gray areas in Figure 1) and the total number of residues, respectively. If $f = g$, there are no further suppressed peaks caused by fluctuation motions in the transmembrane α-helices near the surface areas, as seen for [1-^{13}C]Val- and Ile-bR, (Table 1). If $f < g$, on the other hand, more ^{13}C NMR signals than those of the surface areas could be suppressed by interference of the incoherent fluctuation frequencies (10^4 Hz) with the coherent frequency of the magic angle spinning (50), as demonstrated for [1-^{13}C]Gly-, Ala-, Leu-, Phe-, Trp-labeled bR.

The completely or partially suppressed peaks (in the absence of Mn^{2+}) are related to the presence of such low frequency, *residue-specific dynamics,* in relation to the possibility of conformational fluctuations caused by the time-dependent deviation from the torsion angles corresponding to the lowest energy minimum of a particular conformation. Naturally, such conformational space which allows fluctuation motions

may be limited to a very narrow area for the Val or Ile residues with bulky side-chains at C_α, together with limited χ_1 rotation around the C_α-C_β bond in the C_α-C_βH(X)(Y) moiety in the peptide unit where X and Y are substituents at C_β. This minimum may be very shallow, however, for Gly, Ala, or Leu residues in view of the expected, widely allowed conformational space. Therefore, it is plausible that the above-mentioned low frequency, *residue-specific* backbone dynamic with a fluctuation frequency of 10^4 Hz interferes with the frequency of the magic angle spinning for the [1-^{13}C]Ala, Leu, Phe and Trp residues. The backbone dynamics in these systems could be coupled with a possible rotational motion of the χ_1 angle around the C_α-C_β bond, as schematically represented by the C_α-$C_\beta H_2$-Z system where Z is H, isopropyl, phenyl, or the indole group.

Accordingly, the recommended probes to yield correctly the ^{13}C NMR signals of incorporated ^{13}C-labeled nuclei are [3-^{13}C]Ala, [1-^{13}C]Val or Ile (51).

SURFACE STRUCTURES OF BR

Surface structures of bR, if any, could be easily modified by a variety of intrinsic or environmental factors during the course of crystallization leading to 2D or 3D crystals. Such factors are temperature, pH, ionic strength, crystallographic contact, etc. (28, 33).The C-terminal residues, 226-235, participate in the formation of the C-terminal α-helix (39) protruding from the cytoplasmic surface (as manifested by the peak-position of 15.91 ppm for [3-^{13}C]Ala-bR and also for the Ala C_α and C=O ^{13}C NMR peaks from the helix G'(see Figure 1). This applies to the above-mentioned conformation-dependent ^{13}C chemical shifts (28,29,45,46). Only part of this α-helix, however, is visible by X-ray diffraction (52) owing to the presence of the fluctuation

motions with correlation times of the order of 10^{-6} s at ambient temperature, as judged from the carbon spin-lattice relaxation times, T_1^C, and spin-spin relaxation times, T_2^C, under CP-MAS conditions (39). The involvement of Ala 228 in the C-terminal α-helix was also shown by the obviously reduced peak-intensities of A228G at 15.91 ppm, both in the CP-MAS and the DD-MAS NMR spectra (53).

Therefore, it is shown that the C-terminal α-helix is held together by the loops at the cytoplasmic surface to form the cytoplasmic surface complex or surface structure, stabilized by formation of salt bridges and metal-mediated linkages, as schematically illustrated by the dotted lines in Figure 3. This structure could be destabilized when environmental factors are changed to such as high ionic strength, low pH or high temperature (53). The surface structures are naturally altered either by site-directed mutations at the C-terminal α-helix (R227Q) or at the loop (A160G, E166G, and A168G), and by the manner of altered cation binding, as viewed from the ^{13}C chemical shifts of Ala 228 and 233 (C-terminal α-helix), Ala 103 (C-D loop), and Ala 160 (E-F loop). In contrast, the cytoplasmic ends of the B and F helices are found to undergo fluctuation motions of the order of 10^{-5} s when such a surface structure is disrupted (54). To make proton uptake efficient during the photocycles, the following surface structure is proposed: the C-terminal α-helix of the wild type at ambient temperature is tilted toward the direction of the B and F helices. This facilitates efficient proton uptake by preventing unnecessary fluctuations of the helices. Such a surface structure, however, is destabilized in that the C-terminal α-helix is straightforwardly extended from the helix G at low temperatures or in an M-like state (54). This view is consistent with the previously published data for the “proton binding cluster” consisting of Asp 104, Glu 166 and Glu 224 (55-57).

It is interesting to note that the role of such a C-terminal α-helix is more important for *pharaonis* phoborhodopsin (*p*pR) than bR for the sake of stabilization of the 2:2 complex formation with its cognate transducer (*p*HtrII) through interaction with cytoplasmic α-helices protruding from the cytoplasmic surface, besides the mutual interaction at the transmembrane α-helices (58,59). As a result, such a C-terminal helix is made visible by x-ray diffraction as a result of complex formation with *p*HtrII (60).

MILLISECOND OR MICROSECOND MOTIONS IN 2D CRYSTAL OF BR

To our dismay, we found out that several ^{13}C NMR peaks of certain amino-acid residues could be suppressed depending upon their sites, and the manner of sample preparation when the ^{13}C NMR spectra of fully hydrated bR were recorded at ambient temperature. Thus structural information from such sites could be obscured. Therefore, closer examination of such suppressed signals obviously provides an unrivaled means to evaluate the presence and location of millisecond or microsecond motions for such sites.

The expected ^{13}C NMR line width $1/\pi T_2^C$ under CP-MAS or DD-MAS NMR conditions depends strongly on the incoherent frequency of any fluctuation motion, if it is interfered with either by the coherent frequency of the proton decoupling or by the magic angle spinning. (50,61). In such cases, the overall relaxation rate $1/T_2^C$ can be dominated by the second or third terms given in equation (3) instead of the first term which is applicable to the static component,

$$1/T_2^C = (1/T_2^C)^S + (1/T_2^C)^M{}_{DD} + (1/T_2^C)^M{}_{CS} \qquad (3)$$

where $(1/T_2^C)^S$ is the transverse component due to static C-H dipolar interactions, and $(1/T_2^C)^M{}_{DD}$ and $(1/T_2^C)^M{}_{CS}$ are the transverse components due to the fluctuation of the dipolar and chemical shift interactions in the presence of internal fluctuation motions,

respectively. The latter two terms are given as a function of the correlation time τ_c by

$$(1/T_2^C)^M_{DD} = \Sigma(4\gamma_I^2\gamma_S^2h^2/15r^6)\, I(I+1)\, (\tau_c/(1 + \omega_I^2\tau c^2)) \quad (4)$$

$$(1/T_2^C)^M_{CS} = (\omega_0^2\delta^2\eta^2/45)\, (\tau_c/(1 + 4\omega_r^2\tau_c^2) + 2\tau_c/(1 + \omega_r^2\tau_c^2)) \quad (5)$$

Here. ω_I and ω_S are the gyromagnetic ratios of the I and S nuclei, respectively, and *r* is the internuclear distance between spins *I* and *S*. ω_o and ω_I are the carbon resonance frequency and the amplitude of the proton decoupling RF field, respectively. ω_r is the rate of spinner rotation. δ is the chemical shift anisotropy and η is the asymmetric parameter of the chemical shift tensor.

As far as carbonyl groups with large chemical shift anisotropies are concerned, a decoupling field of 50 kHz is sufficient to reduce the static component at a magnetic field of 9 *T* and the $(1/T_2^C)^M_{CS}$ term will be dominant in the overall value of $1/T_2^C$, while CH_2 or CH_3 signals are determined by the $(1/T_2^C)^M_{DD}$ term alone. It is expected that the C_α signal could be affected by both the $(1/T_2^C)^M_{DD}$ and $(1/T_2^C)^M_{CS}$ terms, depending upon the frequency range of either 50 kHz (ω_I) or 4 kHz (ω_r), respectively. Of course, it is possible to avoid the above-mentioned interference with a frequency of the order of 10^{-4} s by increasing the spinning rate up to 20 kHz.

These considerations provide unique means for a model-free evaluation of such fluctuation frequencies, if the fully visible ^{13}C NMR spectra are available as reference spectra for further evaluation. It is noticed that there exist local fluctuation motions in certain locations even for bR from a 2D crystalline lattice (PM): correlation times for such fluctuation motions for the loops, C-terminal α-helix, and N- and C-terminal ends are 10^{-4} s, 10^{-6} s and 10^{-8} s. These are obtained from the suppressed peaks interfered by the MAS frequency, relaxation parameters, and from the suppressed peaks in the CP-MAS NMR spectra, respectively. However, the frequency for the transmembrane

α-helices is estimated as 10^{-2} s for the 2D crystal as found by a chemical exchange process reflecting the presence of the crystalline lattice as summarized in Figure 3 (39). Indeed, the correlation time for the loops is estimated to be of the order of 10^{-4} s, because the ^{13}C NMR signals of [1-^{13}C]Ala-bR from such region are suppressed by interference of the fluctuation frequency by the magic angle spinning, as already described (39). Such backbone dynamics of the loops is also evaluated by examination of site-specific ^{13}C-^{1}H dipolar couplings in [3-^{13}C]Ala-bR, yielding slow or intermediate frequency motions (62). Naturally, the above-mentioned surface structure of the cytoplasmic complex is far from a static picture. The structure undergoes fluctuations of in the order of 10^{-4} to 10^{-6} s as found by taking into account of the estimated correlation times of its constituent components.

A particular portion of the transmembrane α-helices acquires fluctuation motions with a correlation time of up to 10^{-5} s, leading to suppressed peaks for [3-^{13}C]Ala-bR due to a failure of the peak-narrowing by proton decoupling (61). This occurs when a 2D crystalline lattice is either instantaneously or permanently distorted or is disrupted by removing retinal (41), reconstitution in a lipid bilayer (63), a modified lipid-protein (64), retinal-protein interactions (41), or the M-like state of D85N mutant of bR (65). This kind of dynamic picture, however, has never been seriously taken into account for the data available at cryo-temperatures.

INDUCED PROTEIN DYNAMICS OF BR IN A DISTORTED OR DISRUPTED LATTICE

It is noteworthy that the ^{13}C NMR signals of the loops and some transmembrane α-helices of [3-^{13}C]Ala-bR which resonate at 16.1-16.4 ppm are either completely or

substantially suppressed, respectively, when the ^{13}C NMR signals are recorded in a lipid bilayer in which bR is present as a monomer (63) (Figures 4A and B), as compared with those from bR in a 2D crystalline lattice (Figures 4C and D). This is obviously caused by acquired low-frequency fluctuation motions (10^5 Hz) in the absence of the helix-helix contact due to a disrupted 2D crystalline lattice (see Figure 3) interfering with the proton decoupling frequency (61). Therefore, the backbone dynamics could be modified when the 2D lattice assembly is similarly distorted or disrupted, as in bacterio-opsin (bO) prepared from either hydroxylamine-treated bR or the retinal-deficient E1001 strain in which the helix-helix interactions are substantially modified due to lack of retinal (64). The same applies applies to W80L or W12L mutants in which the side chain of one of two Trp residues, which is oriented outward from the transmembrane α-helices at the interface of the lipid-protein interaction, is absent (64). Therefore, very similar spectral changes are induced for the ^{13}C NMR spectra of [3-^{13}C]Ala- bO, W80L and W12L, except for the presence of one of the loop signals for [3-^{13}C]Ala-bO (41). The resulting characteristic spectral changes are summarized in Table 2, showing the presence or absence of the loop signals. As a measure of the suppressed ^{13}C NMR of the transmembrane α-helices, the intensity ratio of the transmembrane α-helical peak at 16.4 ppm ($I_{16.4}$) vs. the C-terminal α-helix at 15.9 ppm ($I_{15.9}$) varies from 1.2 to 0.4, depending upon the type of ^{13}C-labeled preparation. Further, it was shown that the ^{13}C NMR spectra of some of the [1-^{13}C]Val-labeled proteins are almost completely suppressed in the distorted or disrupted lattice (Table 2). These changes are interpreted in terms of the presence of such a distorted or disrupted 2D lattice, which leads to slow fluctuation motions with a correlation time of 10^{-5} s for the cytoplasmic ends of the helix B and F as deduced from

the reduced peak at 16.4 ppm due to Ala 39 and 168, as compared with a time of 10^{-2} s in the 2D crystalline sample. The acquisition of this kind of motional freedom can be well recognized by the fact that the helices B and F are located either at the interior of the trimer or the outer boundary of the trimeric structure (22) which plays an important role in the helix-helix interaction. Here, it is mentioned that the trimeric structure is preserved for W12L but is disrupted for W80L as judged from the observed CD spectra (64).

This finding suggests that the fluctuation motion of bR with a correlation time of the order of 10^{-2} s in the 2D crystal (30,31) could be accelerated for the rest of the connecting transmembrane α-helices in a distorted or disrupted lattice (Figure 3). Indeed, it is possible to visualize such an accelerated backbone motion with a correlation time of the order of 10^{-4} s (or fluctuation frequency of 10^4 Hz) for the transmembrane α-helices from the suppressed ^{13}C NMR spectra of the [1-^{13}C]Val-labeled proteins (64,65). The loop ^{13}C NMR signals of [3-^{13}C]Ala-D85N are completely suppressed at pH 10. This is concomitant with the taking of the M-like state. In fact, a significant dynamic change is induced together with deprotonation of the Schiff base (SB) at this pH, leading to the deletion of the salt bridge with Asp 85 as a structural constraint as encountered in bO (48,49). However it is cautioned that the resulting spectral features of the [3-^{13}C]Ala proteins could not be distinguished even between bR and the D85N mutant as far as they were examined in the lipid bilayer (65).

In particular, D85N acquires local fluctuation motions with a frequency of 10^4 Hz in the transmembrane B α-helix in the M-like state as manifested from the suppressed ^{13}C NMR signal of the [1-^{13}C]Val-labeled Val 49 residue (49). The local dynamics of D85N at Pro 50 with Val 49 as its neighbor turn out to be unchanged, irrespective of the

charged state of SB as viewed from the ^{13}C NMR spectra of Pro 50 in [1-^{13}C]Pro-labeled D85N (49,66). This means that the transmembrane B α-helix is able to acquire a fluctuation motion with a frequency of 10^4 Hz beyond the kink at Pro 50 in the cytoplasmic side, as schematically illustrated in Figure 5. Concomitantly, a fluctuation motion at the C-helix with a frequency of the order of 10^4 Hz is found to be prominent, due to deprotonation of SB at pH 10, as viewed from the suppressed ^{13}C NMR signal of Pro 91. Accordingly, a novel mechanism as to proton uptake and transport is proposed on the basis of a dynamic aspect such that a transient environmental change from a hydrophobic to a hydrophilic nature at Asp 96 and SB is responsible for the reduced pK_a which makes a proton uptake efficient as a result of the fluctuation motion at the cytoplasmic side of the transmembrane B and C α-helices.

It is also interesting to note that the ^{13}C NMR peak of the C-terminal α-helix was displaced to low frequencies due to the disrupted cytoplasmic complex owing to the removal of salt bridges and metal ions. Consequently, such a surface structure is stabilized when blue membranes are prepared by either complete removal of surface-bound cations (deionized blue) or the neutralization of surface charge by a lowered pH to 1.2 (acid blue) (35). As a result, the accompanying low frequency motions lead to suppressed ^{13}C NMR signals from the loop. Partial neutralization of the Glu and Asp residues at the extracelular side such as E194Q/E204Q (2Glu), E9Q/ E194Q/E204Q (3Glu), and E9Q/E74Q/ E194Q/E204Q (4Glu) also causes global fluctuation motions at these loop regions as well as in the disorganized trimeric form (67). It turns out that these changes at the extracellular side do not strongly affect the protein dynamics as described above.

CONCLUSION AND IMPLICATION OF DYNAMIC PICTURES FOR OTHER MEMBRANE PROTEINS

We have found that several degrees of fluctuation motion, fast and slow motions, are present in bR in the 2D crystalline state, depending upon the particular sites of bR. Well-resolved ^{13}C NMR spectra are fully visible at ambient temperature as far as [3-^{13}C]Ala- or [1-^{13}C]Val-labeled bR are concerned, although the ^{13}C NMR signals from the surface areas including loops and transmembrane α-helices near the surface (8.7Å depth) are suppressed for the preparations labeled with [1-^{13}C]Gly, Ala, Leu, Phe, Tyr, etc. due to interference between the frequency of the fluctuation motions and the frequency of the magic angle spinning. Even in the case of [3-^{13}C]Ala or [1-^{13}C]Val-labeled bR, ^{13}C NMR signals from the loops and transmembrane α-helices are also suppressed when bR is reconstituted in the lipid bilayer owing to the acquired fluctuation frequency which interferes with the frequency of the proton decoupling. This possibility should always be taken into account when the NMR spectra of any kind of membrane proteins are examined as monomers or oligomers in lipid bilayers. In order to achieve maximum peak-intensity and spectral resolution, a low temperature study leading to a 2D array is very helpful if specific lipids arising from expression from *Halobacteria* are present with bR (65).

A dynamic picture of the surface structure or cytoplasmic complex of bR from PM, consisting of the C-terminal α-helix and nearby loops, is well characterized by careful analysis of the ^{13}C NMR spectra, especially those obtained by DD-MAS NMR. The C-terminal α-helix is also present in *p*pR which is directly involved in the complex formation with a cognate transducer (58,59,68,69). In particular, the C-terminal residues of *p*pR, protruding from the cytoplasmic surface, consist of the C-terminal α-helix stem

and tip regions, in addition to the randomly coiled terminal. The latter tip region in *p*pR is in direct contact with the cytoplasmic α-helix of *p*HtrII(1-159) which provides stabilization, as well as the mutual helix-helix interaction which is stabilized by hydrogen bonds between the transmembrane α–helices (Kawamura et al., to be published). This interaction, however, is destabilized in D75N with a *p*HtrII(1-159) complex as a photo-activated state. Therefore, Kawamura et al. proposed that a switching of pairs in the helix-helix interaction occurs from *p*HtrII-*p*pR (59) to *p*HtrII itself when *p*pR is converted to an activated state (D75N). These conformational and dynamical changes of *p*pR and *p*HtrII are related to the transmission of a signal to *p*HtrII (68). Further, it has been demonstrated that the surface structure of ppR, consisting of the C-terminal α-helix and E-F loop, is directly involved in the stabilization of the complex (68).

E. coli diacylglycerol kinase (DGK) is a membrane enzyme which catalyzes the conversion of diacylglycerol to phosphatic acid in membranes. Yamaguchi et al. have showed that the ^{13}C NMR spectra of [3-^{13}C]Ala-, [1-^{13}C]Val-labeled DGK are broadened to yield rather featureless peaks at physiological temperatures, both in DM solution and in lipid bilayers in the liquid crystalline phase. This is due to interference of the motional frequencies of DGK with the frequencies of magic angle spinning or proton decoupling (10^4 or 10^5 Hz, respectively) (69). Distinct ^{13}C NMR signals for up to six peaks, however, are well resolved due to the absence of such fluctuation motions in the gel-phase lipids, for the domains for the transmembrane and amphipathic α-helices and loops. This finding again indicates that acquisition of such low frequency motions with time scales of microseconds to milliseconds is essential for the protein backbone to facilitate the efficient enzymatic activity of DGK. The individual DGK monomers at

physiological temperature are not always tightly packed as anticipated from the trimeric form but are loosely held together in order to allow the backbone fluctuations, even though they could be tightly packed reflecting the dynamic state of the surrounding lipids in the gel phase lipid.

These findings clearly indicate that the presence of slow fluctuation motions with correlation times of 10^{-4} to 10^{-5} s plays an essential role in their respective biological activities, although such motions could be a serious obstacle as viewed from the detailed analysis of the 3D structure at ambient temperature.

ACKNOWLEDGEMENT

The authors are grateful to Professors J. K. Lanyi, Richard Needleman, Esteve Padrós, N. Kamo and James U. Bowie for cooperative works and stimulating discussions.

REFERENCES

1. Blaurock, A. E. and W. Stoeckeneus (1971) Structure of the purple membrane. *Nature New Biology*. **233**, 152-155.
2. Baldwin, J. M., R. Henderson, E. Beckman, and F. Zemlin (1988) Images of purple membrane at 2.8 Å resolution obtained by cryo-electron microscopy. *J. Mol. Biol.,* **202**, 586-591.
3. Grigorieff, N., T. A. Ceska, K. H. Downing, J. M. Baldwin and R. Henderson (1996) Electron-crystallographic refinement of the structure of bacteriorhodopsin. *J. Mol. Biol*. **259**, 393-421.
4. Pebay-Peyroula, E., G. Rummel, J. P. Rosenbusch, and E. M. Landau (1997) X-ray structure of bacteriorhodopsin at 2.5 angstroms from microcrystals grown in lipidic cubic phases. *Science* **277**, 1676-1681.
5. Luecke, H., H. T. Richter, and J. K. Lanyi (1998) Proton transfer pathways in bacteriorhodopsin at 2.3 angstrom resolution. *Science* **280**, 1934-1937.
6. Essen, L., R. Siegert, W. D.Lehman, and D. Oesterhelt (1998) Lipid patches in membrane protein oligomers: crystal structure of the bacteriorhodopsin-lipid complex. *Proc. Natl. Acad. Sci. USA* **95**, 11673-11678.
7. Sato, H., K. Takeda, K. Tani, T. Hino, T. Okada, M. Nakasako, N. Kamiya, and T. Kouyama (1999) Specific lipid-protein interactions in a novel honeycomb lattice structure of bacteriorhodopsin. *Acta. Crystallogr.* **D 55**, 1251-1256.
8. Havelka, W. A., R. Henderson, J. A. Heymann and D. Oesterhelt (1993) Projection structure of halorhodopsin from *Halobacterium halobium* at 6 Å resolution obtained by electron cryo-microscopy. *J. Mol. Biol.* **234**, 837-46.
9. Kolbe, M., H. Besier, L. –O. Essen, and D. Oesterhelt (2000) Structure of the

light-driven chloride pump halorhodopsin at 1.8 Å resolution. *Science* **288**, 1390-1396.

10. Kunji, E. R. S., E. N. Spudich, R. Grisshammer, R. Henderson and J. L. Spudich. (2000) Electron crystallographic analysis of two-dimensional crystals of sensory rhodopsin II: a 6.9 Å projection structure. *J. Mol. Biol*. **308**, 279-293.
11. Luecke, H., B. Shobert, J. K. Lanyi, E. N. Spudich, and J. L. Spudich, (2001) Crystal structure of sensory rhodopsin II at 2.4 angstroms: insights into color tuning and transducer interaction. *Science* **293**, 1499-1503.
12. Royant, A., P. Nollert, K. Edman, R. Neutze, E. M. Landau, E. Pebay-Peyroula, and J. Navaro (2001) X-ray structure of sensory rhodopsin II at 2.1-Å resolution. *Proc. Natl. Acad. Sci. USA* **98**, 10131-10136.
13. Deisenhofer, J., O. Epp, K. Miki, R. Huber, and H. Michel (1985) Structure of the protein subunits in the photosynthetic reaction centre of *Rhodopseudomonas viridis* at 3Å resolution. *Nature* **318**, 618 – 624.
14. Kuhlbrandt, W., D. N. Wang, and Y. Fujiyoshi (1994) Atomic model of plant light-harvesting complex by electron crystallography. *Nature* **367**, 614-621.
15. McDermott, G., S. M. Prince, A. A. Freer, A. M. Hawthornthwaite-Lawless, M. Z. Papiz, R. J. Cogdell, and N. W. Isaacs (1995) Crystal structure of an integral membrane light-harvesting complex from photosynthetic bacteria. *Nature* **374**, 517-521.
16. Iwata, S., C. Ostermeier, B. Ludwig, and H. Michel (1995) Structure at 2.8 Å resolution of cytochrome c oxidase from *Paracoccus denitrificans*. *Nature* **376**, 660-669.
17. Tsukihara, N., H. Aoyama, E. Yamashita, T. Tomizaki, H. Yamaguchi, K.

Shinzawa-Itoh, R. Nakashima, R. Yano and S. Yoshikawa (1995) Structures of metal sites of oxidized bovine heart cytochrome c oxidase at 2.8 Å. *Science* **269**, 1069-1074.

18. Doyle, D. A., J. M. Cabral, R. A. Pfuetzner, A. Kuo, J. M. Gulbiss, S. L. Cohen, B. T. Chait, and R. MacKinnon (1998) The structure of the potassium channel: molecular basis of K^+ conduction and selectivity. *Science* **280**, 69-77.
19. Chang, G., R. H. Spencer, A.T. Lee, M.T. Barclay, and D. C. Rees. (1998) Structure of the MscL homolog from Mycobacterium tuberculosis: a gated mechanosensitive ion channel. *Science* **282**, 2220-2226.
20. Palczewski, K., T. Kumasaka, T. Hori, C. A. Behnke, H. Motoshima, B. A. Fox, I. Le Trong, D. C. Teller, T. Okada, R. E. Stenkamp, M. Yamamoto, and M. Miyano (2000) Crystal structure of rhodopsin: A G protein-coupled receptor. *Science* **289**, 739-745.
21. Toyoshima, C., M. Nakasako, H. Nomura, and H. Ogawa (2000) Crystal structure of the calcium pump of sarcoplasmic reticulum at 2.6 A resolution. *Nature* **405**, 647-655.
22. Krebs, M. P. and T. A. Isenbarger (2000) Structural determinants of purple membrane assembly. *Biochim. Biophys. Acta* **1460**, 15-26.
23. Dencher, N. A., M. P. Heyn (1983) Bacteriorhodopsin monomers pump protons. *FEBS Lett*. **108**, 307-310.
24. Dencher, N. A., K. -D. Kohl, and M. P. Heyn (1983) Photochemical cycle and light-dark adaptation of monomeric and aggregated bacteriorhodopsin in various lipid environments. *Biochemistry* **22**, 1323-1334.
25. Milder, S. J., T. E. Thorgeirsson, L. J. Mierke, R. M. Stroud, and D. S. Kliger (1991)

Effects of detergent environments on the photocycle of purified monomeric bacteriorhodopsin. *Biochemistry* **30**, 1751-1761.

26. Dencher, N. A., and M. P. Heyn (1982) Preparation and properties of monomeric bacteriorhodopsin. *Methods Enzymol*. **88**, 5-10.

27. Varo, G., and J. K. Lanyi (1991) Effects of the crystalline structure of purple membrane on the kinetics and energetics of the bacteriorhodopsin photocycle. *Biochemistry* **30**, 7165-7171.

28. Saitô, H., S. Tuzi, S. Yamaguchi, M. Tanio, and A. Naito (2000) Conformation and backbone dynamics of bacteriorhodopsin revealed by ^{13}C-NMR. *Biochim. Biophys. Acta* **1460**, 39-48.

29. Saitô, H., S. Tuzi, M. Tanio and A. Naito (2002) Dynamic aspects of membrane proteins and membrane-associated peptides as revealed by ^{13}C NMR: Lessons from bacteriorhodopsin as an intact protein. *Annu. Rep. NMR Spectrosc*. **47**, 39-108

30. Saitô, H. (2004) Dynamic pictures of membrane proteins in two-dimensional crystal, lipid bilayer and detergent as revealed by site-directed solid-state ^{13}C NMR. *Chem. Phys. Lipids.* **132**, 101-112.

31. Saitô, H. (2006) Site-directed solid-state NMR on membrane proteins. *Annu. Rep. NMR Spectrosc.* **57**, 99-175

32 Saitô, H., I. Ando and A. Naito. (2006) *Solid state NMR spectroscopy for biopolymers: Principles and applications*. Springer, Dordrecht, The Netherland, chapter 13.

33 Heymann, J. B., D. J. Muller, E. M. Randau, J. P. Rosenbusch, E., Pebay-Peyroula, G. Büldt, and A. Engel (1999) Charting the surfaces of the purple membrane. *J. Struct. Biol*. **128**, 243-249.

34 Müller, D. J., H.-J. Sass, S. A. Müller, G. Büldt, and A. Engel (1999) Surface structures of native bacteriorhodopsin depend on the molecular packing arrangement in the membrane. *J. Mol. Biol*. **285**, 1903-1909.

35 Tuzi, S., S. Yamaguchi, M. Tanio, H. Konishi, S. Inoue, A. Naito, R. Needleman, J. K. Lanyi, and H. Saitô (1999) Location of a cation-binding site in the loop between helices F and G of bacteriorhodopsin as studied by ^{13}C NMR. *Biophys. J*. **76**, 1523-1531.

36 Tuzi, S., A. Naito and H. Saitô (1993) A high-resolution solid-state ^{13}C-NMR study on [1-^{13}C]Ala and [3-^{13}C]Ala and [1-^{13}C]Leu and Val-labelled bacteriorhodopsin. Conformation and dynamics of transmembrane helices, loops and termini, and hydration-induced conformational change. *Eur J Biochem*. **218**, 837-844.

37 Fitter, J., R. E. Lechner and N. A. Dencher (1999) Interactions of hydration water and biological membranes studied by neutron scattering. *J. Phys. Chem.* B, **103**, 8036-8050

38 Dencher, N. A., H. J. Sass and G. Büldt (2000) Water and bacteriorhodopsin: structure, dynamics and function. *Biochim. Biophys. Acta* **1460**, 192-203.

39 Yamaguchi, S., S. Tuzi, K. Yonebayashi, A. Naito, R. Needleman, J. K. Lanyi, and H. Saitô (2001) Surface dynamics of bacteriorhodopsin as revealed by ^{13}C NMR studies on [^{13}C]Ala-labeled proteins: Detection of millisecond or microsecond motions in interhelical loops and C-terminal α-helix. *J. Biochem*. *(Tokyo)* **129**, 373-382.

40 Tuzi, S., A. Naito, and H. Saitô (1996) Conformation and dynamics of [3-^{13}C]Ala-labeled bacteriorhodopsin and bacterioopsin, induced by interaction with retinal and its analogs, as studied by ^{13}C nuclear magnetic resonance. *Biochemistry* **35**,

7520-77527.

41 Yamaguchi, S., S.Tuzi, M. Tanio, A. Naito, J. K. Lanyi, R. Needleman and H. Saitô (2000) Irreversible conformational change of bacterio-opsin induced by binding of retinal during its reconstitution to bacteriorhodopsin, as studied by ^{13}C NMR. *J. Biochem.* **127**, 861-869.

42 Solomon, I. (1955) Relaxation processes in a system of two spins. *Phys. Rev*. **99**, 559-565

43 Bloembergen, N. (1957) Proton relaxation times in paramagnetic solution. *J. Chem. Phys*. **27**, 572-573

44 Tuzi, S., J. Hasegawa, R. Kawaminami, A. Naito, and H. Saitô (2001) Regio-selective detection of dynamic structure of transmembrane α-helices as revealed from ^{13}C NMR spectra of [3-^{13}C]Ala-labeled bacteriorhodopsin in the presence of Mn^{2+} Ion. *Biophys J*, **81**, 425-434.

45 Saitô, H. (1986) Conformation-dependent ^{13}C chemical shifts: A new means of conformational characterization as obtained by high-resolution solid-state NMR, *Magn. Reson. Chem*. **24**, 835-852.

46 Saitô, H. and I. Ando (1989) High-resolution slid-state NMR studies on synthetic 48 and biological macromolecules. *Annu. Rep. NMR Spectrosc*. **21**, 209-290.

47 Krimm, S. and A. M. Dwivedi (1982) Infrared spectrum of the purple membrane: clue to a proton conduction mechanism? *Science* **216**, 407-408.

48 Kawase. Y., M. Tanio, A. Kira, S. Yamaguchi, S. Tuzi, A. Naito, M. Kataoka, J. K. Lanyi, R. Needleman and H. Saiô (2000) Alteration of conformation and dynamics of bacteriorhodopsin induced by protonation of Asp 85 and deprotonation of Schiff base as studied by ^{13}C NMR. *Biochemistry* **39**,

14472-14480.

49 Kira, A., M. Tanio, S. Tuzi and H. Saitô (2004) Significance of low-frequency local fluctuation motions in the transmembrane B and C α-helices of bacteriorhodopsin, to facilitate efficient proton uptake from the cytoplasmic surface, as revealed by site-directed solid-state ^{13}C NMR. *Eur. J. Biophys*. **33,** 580-588.

50 Suwelack, D., W. P. Rothwell, and J. S. Waugh (1980) slow molecular motion detected in the NMR spectra of rotating solids. *J. Chem. Phys*. **73**, 2559-2569

51 Saito, H., J. Mikami, S. Yamaguchi, M. Tanio, A. Kira, T. Arakawa, K. Yamamoto, and S. Tuzi (2004) Site-directed ^{13}C solid-state NMR studies on membrane proteins: strategy and goals toward revealing conformation and dynamics as illustrated for bacteriorhodopsin labeled with [1-^{13}C]amino acid residues. *Magn. Reson. Chem.* **42**, 218-230.

52 Luecke, H. B. Schobert, H.-T. Richter, J.- P. Cartailler and J. K. Lanyi (1999) Structure of bacteriorhodopsin at 1.55 Å resolution. *J. Mol. Biol*. **291**, 899-911.

53 Yamaguchi, S., K.Yonebayashi, H. Konishi, S. Tuzi, A. Naito, J. K. Lanyi, R. Needleman, and H. Saitô (2001) Cytoplasmic surface structure of bacteriorhodopsin consisting of interhelical loops and C-terminal α helix, modified by a variety of environmental factors as studied by ^{13}C-NMR. *Eur. J. Biochem*. **268**, 2218-2228

54 Yonebayashi, K., S. Yamaguchi, S. Tuzi, and H. Saitô (2003) Cytoplasmic surface structures of bacteriorhodopsin modified by site-directed mutations and cation binding as revealed by ^{13}C NMR. *Eur. Biophys. J*. **32**, 1-11

55 Riesle, J., D. Osterhelt, N. A. Dencher, and J. Heberle (1996) D38 is an essential part of the proton translocation pathway in bacteriorhodopsin. *Biochemistry* **35**,

6635-6643.

56 Checover, S., E. Nachliel, N. A. Dencher, and M. Gutman (1997) Mechanism of proton entry into the cytoplasmic section of the proton-conducting channel of bacteriorhodopsin. *Biochemistry* **36**, 13919-13928.

57 Checover, S., Marantz, E. L. Nachliel, M. Gutman, M.Pfeiffer, J. Tittor, D. Osterhelt, and N. A. Dencher (2001) Dynamics of the proton transfer reaction on the cytoplasmic surface of bacteriorhodopsin. *Biochemistry* **40**, 4281-4292.

58 Arakawa, T., K. Shimono, S. Yamaguchi, S. Tuzi, Y. Sudo, N. Kamo and H. Saitô (2003) Dynamic structure of *pharaonis* phoborhodopsin (sensory rhodopsin II) and complex with a cognate truncated transducer as revealed by site-directed ^{13}C solid-state NMR. *FEBS Lett*. **536**, 237-240.

59 Yamaguchi, S., K. Shimono, Y. Sudo, S. Tuzi, A. Naito, N. Kamo, and H. Saitô (2004) Conformation and dynamics of the [3-^{13}C]Ala, [1-^{13}C]Val-labeled truncated pharaonis transducer, pHtrII (1-159), as revealed by site-directed ^{13}C solid-state NMR: changes due to association with phoborhodopsin (sensory rhodopsin II). *Biophys. J.* ***86****,* 3130-3140.

60 Gordeliy, V. I., J. Labahn, R. Moukhametzianov, R. Efremov, J. Granzin, R. Schlesinger, G. Buldt, T. Savopol, A. J. Scheidig, J. P. Klare, and M. Engerhard (2002) Molecular basis of transmembrane signalling by sensory rhodopsin II-transducer complex. *Nature* **419**, 484-487.

61 Rothwell, W. P. and J. S. Waugh (1981) Transverse relaxation of dipolar coupled spin systems under rf irradiation: detecting motions in solid. *J. Chem. Phys*. **74**, 2721-2732.

62 Barré, P., S. Yamaguchi, H. Saitô and D. Huster (2003) Backbone dynamics of

bacteriorhodopsin as studied by ^{13}C solid-state NMR spectroscopy. *Eur. Biophys. J.* **32**, 578-584.

63 Saitô, H., K. Yamamoto, S. Tuzi, and S. Yamaguchi (2003) Backbone dynamics of membrane proteins in lipid bilayers: the effect of two-dimensional array formation as revealed by site-directed solid-state ^{13}C NMR studies on [3-^{13}C]Ala- and [1-^{13}C]Val-labeled bacteriorhodopsin. *Biochim. Biophys. Acta* **1616**, 127-136.

64 Saitô, H., T. Tsuchida, K. Ogawa, T. Arakawa, S. Yamaguchi, and S. Tuzi (2002) Residue-specific millisecond to microsecond fluctuations in bacteriorhodopsin induced by disrupted or disorganized two-dimensional crystalline lattice, through modified lipid-helix and helix-helix interactions, as revealed by ^{13}C NMR, *Biochim. Biophys. Acta* **1565**, 97-106.

65 Yamamoto, K., S. Tuzi, H. Saitô, I. Kawamura, and A. Naito (2006) Conformation and dynamics changes of bacteriorhodopsin and its D85N mutant in the absence of 2D crystalline lattice as revealed by site-directed ^{13}C NMR. *Biochim. Biophys. Acta* **1758**, 181-189.

66 Tuzi, S., A. Naito and H. Saitô (2003) Local protein structure and dynamics at kinked transmembrane α-helices of [1-^{13}C]Pro-labeled bacteriorhodopsin as revealed by site-directed solid-state ^{13}C NMR. *J. Mol. Struct*. **654**, 205-214.

67 Saitô, H., S. Yamaguchi, K. Ogawa, S. Tuzi, M. Márquez, C. Sanz, and E. Padrós (2004) Glutamic acid residues of bacteriorhodopsin at the extracellular surface as determinants for conformation and dynamics as revealed by site-directed solid-state ^{13}C NMR. *Biophys. J.* **86**, 1673-1681.

68 Kawamura, I., Y. Ikeda, Y. Sudo, M. Iwamoto, K. Shimono, S. Yamaguci, S. Tuzi, H. Saitô, N. Kamo, and A. Naito, (2006) Participation of the surface structure of

pharaonis phoborhodopsin, ppR and its A149S and A149V mutants, consisting of the C-terminal α-helix and E-F loop, in the complex-formation with the cognate transducer *p*HtrII, as revealed by site-directed ^{13}C solid-state NMR, *Photochem. Photobiol*., in press.

69 Yamaguchi, S., S. Tuzi, J. U. Bowie, and H. Saitô (2004) Secondary structure and backbone dynamics of Escherichia coli diacylglycerol kinase, as revealed by site-directed solid-state ^{13}C NMR. *Biochim. Biophys. Acta* **1698**, 97-105.

Table 1 Comparison of relative proportion of the ^{13}C NMR signals from the surface areas of [1-^{13}C]amino-acid labeled bR from purple membrane as estimated from the ^{13}C NMR intensity ratio with(I) and without (I_0) Mn^{2+} ion

	Estimated from ^{13}C signals $(1-I/I_0)$, f	Predicted amounts of residues at the surface Areas (8.7 Å from the membrane surface), g	Suppressed ^{13}C NMR peaks from the surface areas caused by slow motions
Gly	0.14	0.67	suppressed
Ala	ca. 0[a]	0.62	almost completely suppressed
Leu	0.11	0.49	suppressed
Phe	0.24	0.55	suppressed
Trp	0.24	0.38	suppressed
Val	0.41	0.38	none
Ile	0.50	0.56	none

[a] Reference 41

Table 2 Characteristic loop ^{13}C NMR signals[a] and intensity ratio of the transmembrane α-helix at 16.3 ppm ($I_{16.3}$) vs. C-terminal α-helix at 15,9 ppm ($I_{15.9}$)

	bR	W12L	D85N		W80L	bO	bR	bR	D85N
	2D crystal		pH 7	pH 10			deionized	monomer[b]	monomer[b]
Loop C-D (Ala 103)	++	-	+ [c]	-	-	++	-	-	-
E-F (Ala 160)	++	-	+ [c]	-	-	-	-	-	-
F-G (Ala 196)	++	-	+ [c]	-	-	-	-	-	-
$I_{16.3} / I_{15.9}$	1.2	0.9	0.7	0.5	0.7	0.6	0.4	0.4	0.8
^{13}C NMR of [1-^{13}C]Val-labeled proteins	++	-	+	+	-	+	+	-	-
Refs	39	41		51	51	41	47	37	62
64									

[a] ++: fully visible, +: partially suppressed, - : suppressed. [b] in lipid bilayer, [c] displaced also

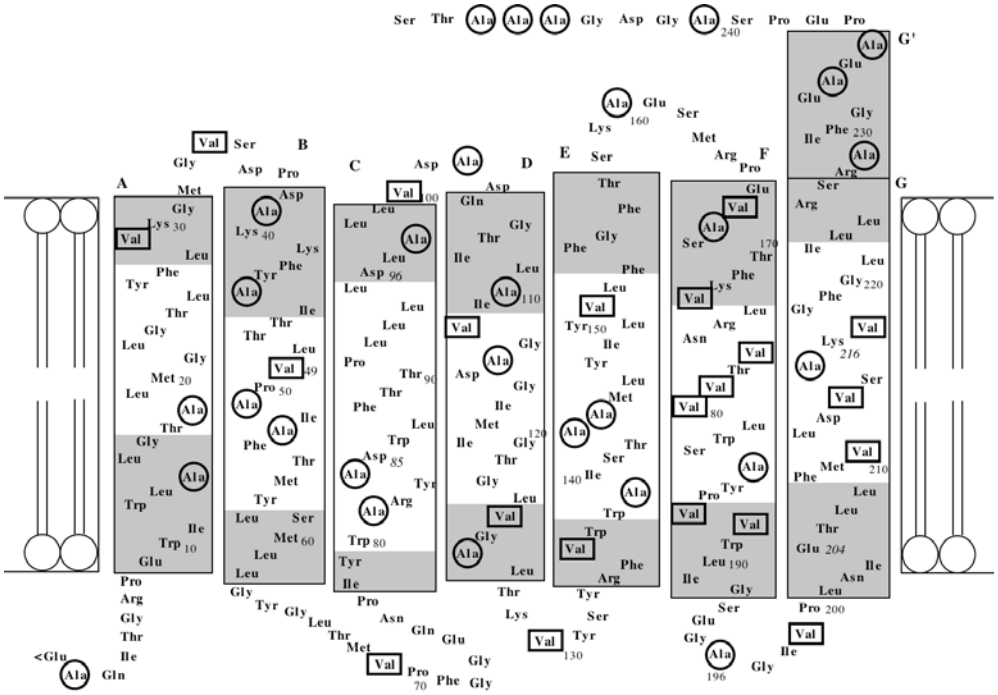

Figure 1 Schematic representation of the secondary structure of bR taking into account of its secondary structure revealed by x-ray diffraction of 3D structure. It consists of the C-terminal α-helix (helix G' protruding from the membrane surface) held together by the C-D and E-F loops to form the surface structure or cytoplasmic complex, together with the seven transmembrane α-helices (A-G) (31). The transmembrane α-helix identified by x-ray diffraction and the C-terminal α-helix revealed by ^{13}C NMR are shown by the boxes. The loops and N- or C-terminus residues, however, are not well defined either by lack of defined electron density or different among published data depending upon the crystallization conditions. The Ala and Val residues are highlighted by the circles and rectangular boxes, respectively.

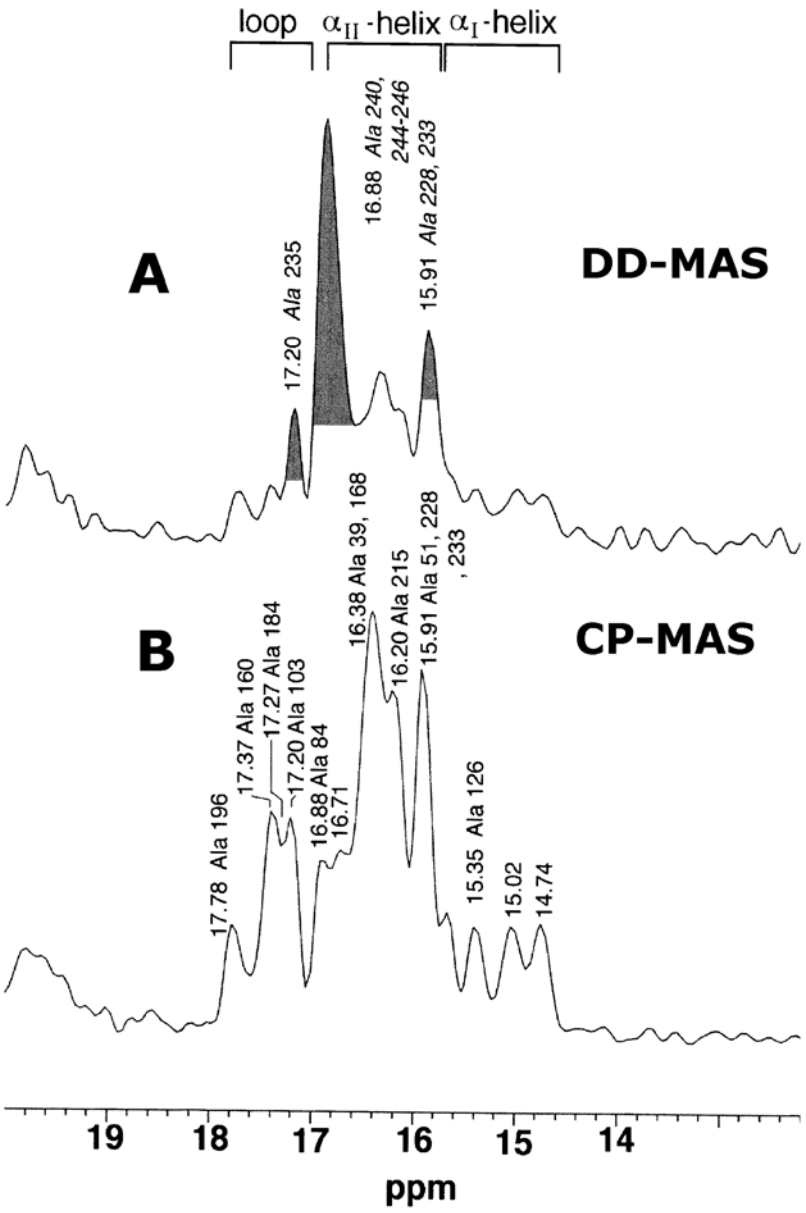

Figure 2 Comparison of the ^{13}C DD-MAS (A) and CP-MAS (B) NMR spectra of [3-^{13}C]Ala-labeled bacteriorhodopsin from the purple membrane (2D crystal). The three peaks marked by gray on the upper trace are from the Ala residues located at the N- and C-terminal moieties (37).

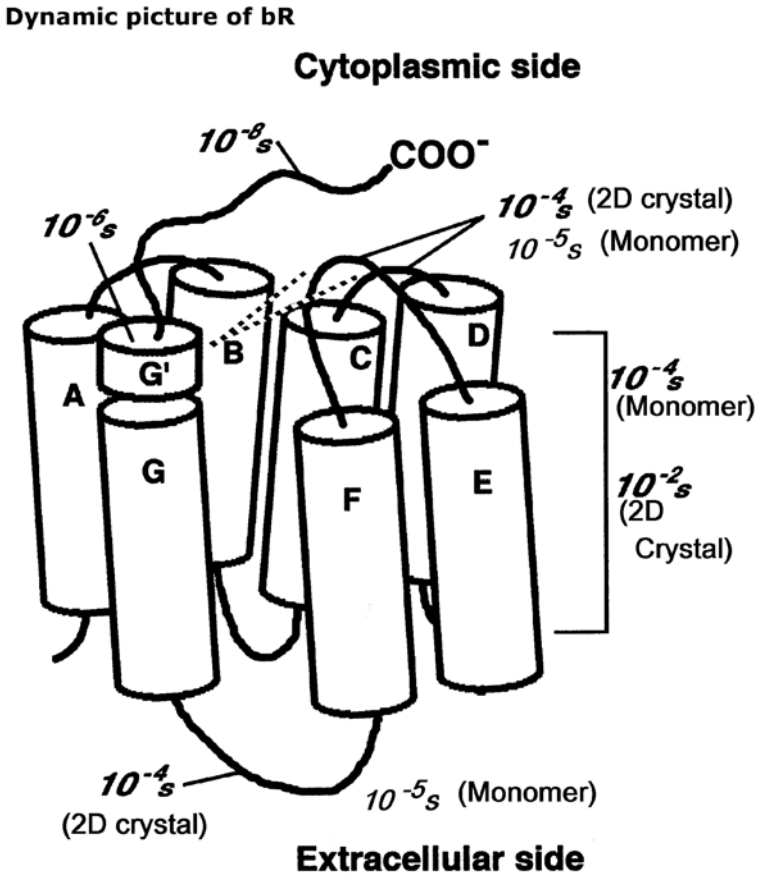

Figure 3 Schematic representation of the secondary structure and dynamics for bR, consisting of the C-terminal α-helix (helix G' protruding from the membrane surface) held together by the C-D and E-F loops to form the surface structure or cytoplasmic complex, together with the seven transmembrane α-helices (A-G) (31). The protein dynamics differs substantially between the 2D crystal and the monomer in the lipid bilayer.

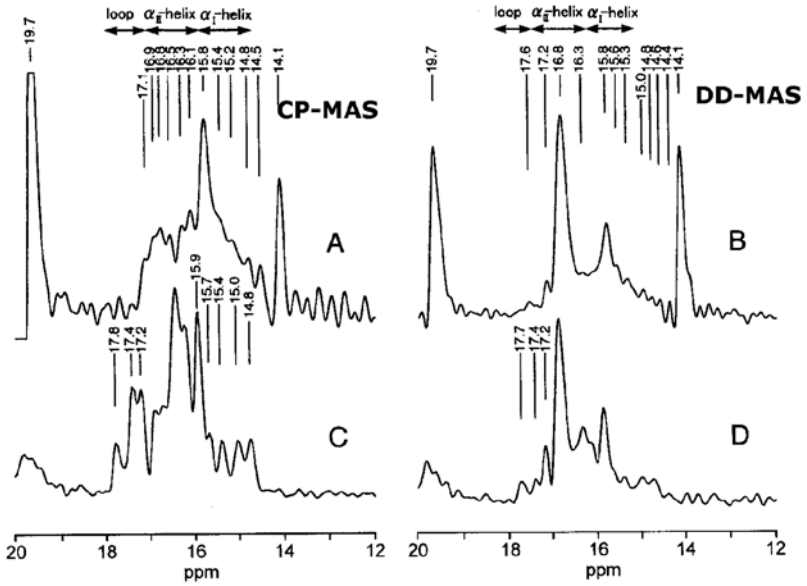

Figure 4 ^{13}C CP-MAS (left) and DD-MAS (right) NMR spectra of [3-^{13}C]Ala-labeled bR reconstituted in an egg PC bilayer (a and b; 1:50 mol ratio) and from PM (c and d). The intense peaks at 19.7 and 14.1 ppm are ascribed to lipid methyl groups from *Halobacteria* and egg PC, respectively (65).

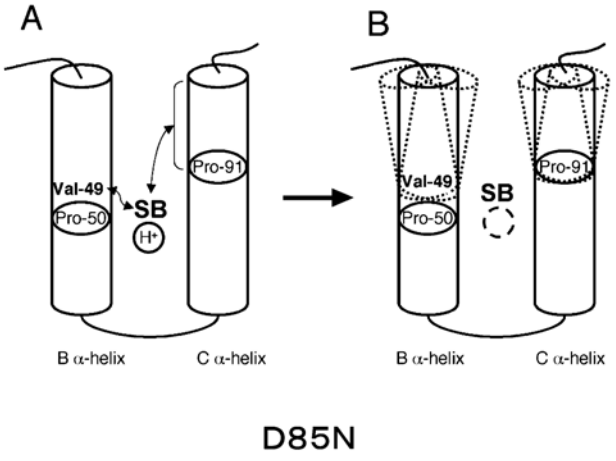

Figure 5 Schematic representation of the dynamic behavior of the B and C α-helices of the D85N mutant, accompanied by protonation of the Schiff base, as viewed from the ^{13}C NMR spectral behavior of Val 49 and Pro 91. A: ground state (pH 7); B: M-like state at pH 10 (52).